J Nanostruct 10(3): 518-530, Summer 2020

RESEARCH PAPER

Synthesis, Characterization and Photocatalytic Activity of $FeCr_2O_4$ and $FeCr_2O_4$/Ag Nanocomposites

Ali Abbasi[1*], Amir Homayoun Keihan[2], Mazyar Ahmadi Golsefidi [3*], Mehdi Rahimi-Nasrabadi[2,4*], Hossein Khojasteh[5]

[1] Students' research committee, Baqiyatallah University of Medical Sciences,Tehran, Iran

[2] Molecular Biology Research Center, Systems Biology and Poisonings Institute, Baqiyatallah University of Medical Sciences, Tehran, Iran

[3] Department of chemistry, Faculty of sciences, Gorgan branch, Islamic Azad University, Gorgan, Iran

[4] Faculty of Pharmacy, Baqiyatallah University of Medical Sciences, Tehran, Iran

[5] Department of Chemistry, Faculty of Science, Soran University, P. O. Box 624, Soran, Kurdistan Regional Government, Iraq

ARTICLE INFO

Article History:
Received 29 February 2020
Accepted 12 May 2020
Published 01 July 2020

Keywords:
Nanostructures
Photodeposition
Photocatalytic degradation
Hydrothermal
$FeCr_2O_4$

ABSTRACT

Ferrite chromite ($FeCr_2O_4$) powders have been synthesized by a hydrothermal method using various alkaline agents and capping agent. For the first time, nanostructured Ferrite chromite was synthesized with utilizing tetraethylenepantamine as a new alkaline agent. The SDS, PVP and PEG as stabilization agent and capping agent in presence of TEPA as alkaline agent were employed to prepare of the Ferrite chromite. The structural character of as-synthesized powders was characterized by X-ray diffraction (XRD), scanning electron microscope (SEM) and energy dispersive X-ray microanalysis (EDX). The results indicate that the as-obtained powders are pure. The electronic properties of as-synthesized powders was characterized by UV–Vis diffuse reflectance analysis (DRS), which shows the as-obtained sample has a significant absorption in the UV region. The photocatalytic degradation of the rhodamine B, methyl orange, murexide and methylene blue as water pollutants were investigated. According to the results, photocatalytic activity of $FeCr_2O_4$/Ag nanostructures were better than of other samples and degradation percent of rhodamine B as a cationic pollutant was more than the other dyes.

How to cite this article
Abbasi A., Keihan AH., Ahmadi Golsefidi M., Rahimi-Nasrabadi M., Khojasteh H. Synthesis, Characterization and Photocatalytic Activity of $FeCr_2O_4$ and $FeCr_2O_4$/Ag Nanocomposites. J Nanostruct, 2020; 10(3): 518-530. DOI: 10.22052/JNS.2020.03.008

INTRODUCTION

Spinel compounds are highly regarded owing to interesting physico-chemical properties and their applications such as super hard materials [1], magnetic materials [2] and high-temperature ceramics [3]. Oxides with spinel structure (with general formula $A^{2+}B_2^{3+}O_4$, in which the A-site is tetrahedrally and the B-site is octahedrally coordinated) are widely used as utile and cheap sensors for detection of toxic and hazardous materials. One of the most important spinel compounds is $FeCr_2O_4$ due to their potential application. $FeCr_2O_4$ has a normal spinel structure that Fe^{2+} and Cr^{3+} ions have a strong preference for the tetrahedral A- and the octahedral B-sites, respectively.

* *Corresponding Author Email: MAIL*

Spinels have been synthesized by various methods such as hydrothermal [4], sonochemical [5], sol–gel [6], thermal decomposition [7], co-precipitation [8] and microemulsion [9] methods. But using the conventional solid-state method at high temperature, spinel particles obtained with low surface areas. Chromite is used mainly in catalytic and photocatalytic processes, for example, $CuCr_2O_4$ and $CoCr_2O_4$ spinel's are operational and active catalysts that are applied for hydrocarbon oxidation [10, 11], $NiCr_2O_4$ can be applied as a catalyst for oxidative dehydrogenation of propane [12] and $ZnCr_2O_4$ can be applied as a photocatalyst.

A large number of chromites have been prepared in nanocrystal form to date. For instance, Some chromites, such as $CuCr_2O_4$, $NiCr_2O_4$, $ZnCr_2O_4$, and $CoCr_2O_4$, have been synthesized using co-precipitation route, by the process of re-crystallization from pyridine followed by ignition in the temperature range of 700–1200 °C, $MgCr_2O_4$ nanocrystals have been synthesized when an appropriate mixture of oxides is pressed into bars and sintered for several hours in an electric furnace at 1400 °C. FeCr2O4 chromite with the spinel structure forms spinel solid solutions with other end-members, $MgCr_2O_4$, $MgAl_2O_4$, $FeAl_2O_4$, etc., in various crustal and upper-mantle rocks. Chromite is also a major chromiumore mineral.

Also chromite compounds were considered as inorganic pigment [13], catalyst or support for a catalyst including the removal of NO_x and diesel soot particulate [14, 15], oxidation of toluene [16], selective reduction of NO with NH_3 [17] and water-gas shift reaction [18]. Chromite nanostructures were synthesized by many routs such as; thermolysis of polymer metal complex [19, 20] hydrothermal synthesis [21], sonochemical technique [22], co-precipitation [23], solution combustion method, ignition of $CoCr_2O_7{\cdot}4C_5H_5N$ precursor [24], sol-gel route with propylene oxide as a gelation agent and low-temperature combustion method using citric acid [25].

Here we report the synthesis, morphology and structure characterization of $FeCr_2O_4$ and $FeCr_2O_4$/Ag nanostructures by hydrothermal method. Here, $N(Et)_3$, NH_3 and tetraethylenepantamine (TEPA) were used as alkaline agents. Also PEG, PVP and SDS were used as capping agent. For investigation photocatalytic activity of nanoparticles were applied of several factors such as various dyes (rhodamine B, methylene blue and methyl orange), different temperature and grain size of $FeCr_2O_4$ nanostructures.

MATERIALS AND METHODS

The materials applied in the present work were $FeCl_2$, $Cr(NO_3)_3$ (Merck, 99.9%), $AgNO_3$, $N(Et)_3$, NH_3, tetraethylenepentamine, SDS, PVP and PEG. All chemicals were used without further purification. Also de-ionized water was used as solvent. Powder X-ray diffraction (XRD) patterns of the as-synthesized $FeCr_2O_4$ nanostructures were recorded by applying a diffractometer of Philips Company with X'PertPromonochromatized Cu Kα radiation (λ= 1.54 Å). Fourier tranform infrared (FT-IR) spectroscopy was obtained as potassium bromide pellets in the range of 400–4000 cm^{-1} with a Nicolet-Impact 400D spectrophotometer. SEM images were taken using an LEO instrument model 1455VP. Prior to taking images, the samples were coated by a very thin layer of Pt (using a BAL-TEC SCD 005 sputter coater) to make the sample surface conductor, to prevent charge accumulation, and to obtain a better contrast. The EDS analysis of the as-produced lead chromate nanostructure was carried out by employing a Philips XL30 microscope. The magnetic properties of the samples were detected at room temperature using a vibrating sample magnetometer. The UV–Vis diffuse reflectance spectrum of the as-produced lead chromate nanostructures was obtained on a UV–Vis spectrophotometer (Shimadzu, UV-2550, Japan). GC-2550TG (Teif Gostar Faraz Company, Iran) were used for all chemical analyses.

Synthesis of $FeCr_2O_4$ nanoparticles

$FeCr_2O_4$ nanoparticles were prepared by the reaction of $FeCl_2$ with chrome nitrate and deionized water as solvent. Here NH_3, $N(Et)_3$ and tetraethylenepentamine were used as alkaline agents. For the investigation of capping agent effect SDS, PVP and PEG were applied. In a typical synthesis, 1 mmol of $FeCl_2$ and 2 mmol of $Cr(NO_3)_3$ powders were dissolved in 40 mL of distilled water. The mixed solution was subsequently added into 30 mL distilled water containing capping agent under stirring. Then, TEPA as alkaline agent was added drop wise to the aqueous solution containing Cr and Fe. Next, the mixture was putted in an autoclave for 10 hours at 180 °C. The formed precipitates were collected and washed with double distilled water and methanol and dried

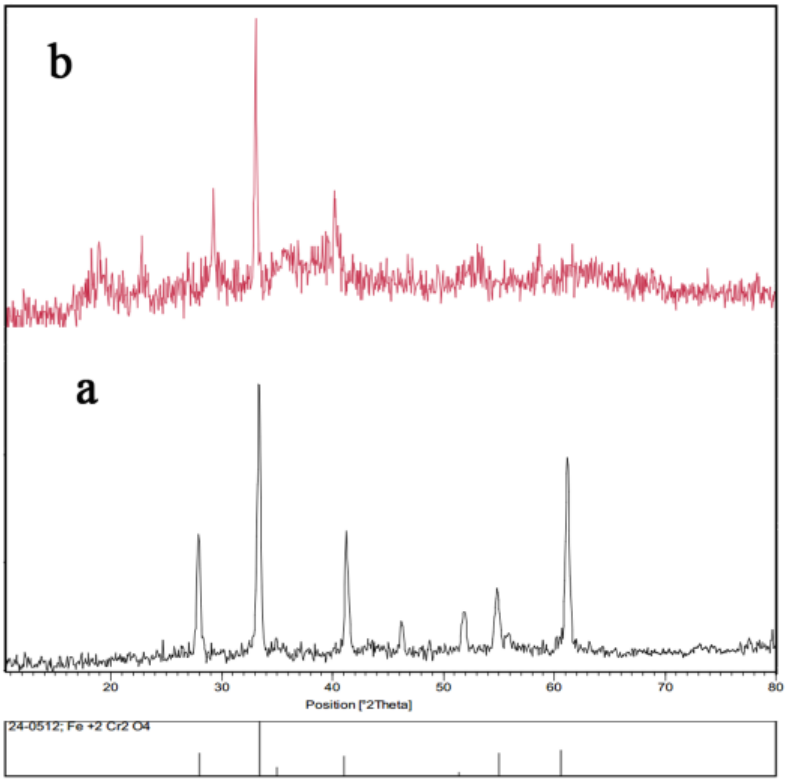

Fig. 1. XRD patterns of (a) $FeCr_2O_4$ calcinated at 700 °C (sample 5) and (b) $FeCr_2O_4$/Ag

at 60 °C. Finally, calcination of the product was carried out at 700 °C for 3h.

Synthesis of $FeCr_2O_4$/Ag nanocomposite

$FeCr_2O_4$/Ag nanocomposite was prepared by using of photodeposition method. First 0.2 gr as-prepared $FeCr_2O_4$ nanostructures dissolved in 50 ml deionized water and then 0.010 $Ag(NO)_3$ were added to resultant solution. The mixture stirred for 30 minutes in ultrasound bath to dispersion magnetic nanoparticles in the solvent. Then the solution was moved to quartz tube and stirred under UV irradiation for 3 hours. Final solid separated, washed with ethanol and water three times and dried at 70 °C.

Photocatalytic measurements

The photocatalytic efficiency of the catalysts was investigated using a 100 ml quartz tube. A suitable amount of the dye solution (initial concentration was 10 ppm) was employed as organic pollution to determine the photocatalytic activity. 0.05 g of catalyst was used for degradation of 40 ml solution. The resulting solution was stirred to obtain the maximum absorption of organic pollutant molecules on the photocatalyst surface and to make oxygen available for the photodegradation reaction and to obtain most homogeneity in the mixture. The solution was irradiated by a 400 W UV lamp which was placed in a quartz pipe in the middle of reactor. It was turned on after 30 min stirring the solution and sampling (about 5-10 ml) was done every 20 min. The samples were filtered and centrifuged to separate the catalyst and after that, samples were analyzed with the UV–Vis spectrometer. The water pollutant photocatalytic degradation percentage was determined as follow;

$$DP(t) = \frac{A_0 - A_t}{A_0} \times 100 \quad (1)$$

Where A_0 and A_t are the concentration of water pollutant at 0 and t min by a UV–Vis spectrometer respectively.

RESULTS AND DISCUSSION

XRD analysis, which is the most useful

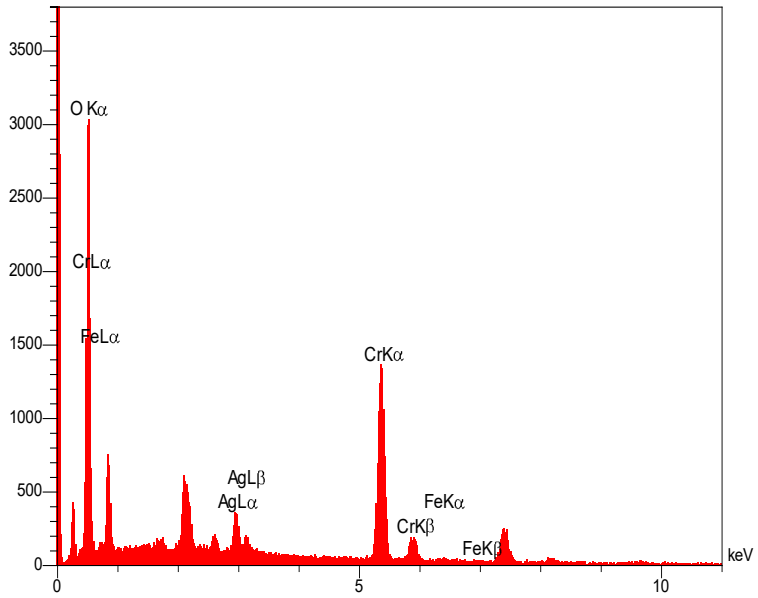

Fig. 2. EDS pattern of $FeCr_2O_4$ /Ag nanostructures

technique for identification of crystalline structure, was employed to study the obtained sample. The crystalline structure of the as-prepared $FeCr_2O_4$ nanostructure was recognized by XRD analysis (Fig 1a). It indicates that the pattern matches the JCPDS 24-0512 file identifying $FeCr_2O_4$ (sample no. 4). The crystalline sizes was calculated using the Scherrer equation, $D_c = \frac{K\lambda}{\beta Cos\theta}$,where Value of K is 0.9 and considered as shape factor, β is full width at half maximum and λ is the X-ray wavelength which usually for Cu K_α radiation to be considered 0.154 nm. Also the average particle size by using of highest peak (3 1 1), FWHM and above equation was estimated~ 57 nm. According to the obtained XRD pattern of the $FeCr_2O_4$/Ag sample calcinated at 700 °C, no specific peak related to Ag observed that this is due to a small amount of silver in the catalyst structure (Fig 1b).

In order to prove the existence of the silver particles on the substrate, elemental analysis (EDS) analysis was applied. This analysis confirms that presence of silver on the surface of $FeCr_2O_4$ nanostructure. This analysis reveals that the elements in this sample are Fe, Cr, Ag and O only (Fig. 2).

The scanning electron microscopy (SEM) images of $FeCr_2O_4$ nanoparticle at different alkaline agent and capping agent was taken and used for synthesis condition optimization. First, the effect of alkaline agent on the particle size and morphology was investigated. Here, we used the NH_3, $N(Et)_3$ and TEPA as alkaline agent. As shown in SEM photographs, when used of the TEPA, we have spherical morphology (Fig. 3 a and b), but when we used the NH_3 (Fig. 3c and d) and $N(Et)_3$ (Fig. 3 e and f), it is clear that the obtained nanoparticles are non-uniform and particle size has been increased. So the best alkaline agent obtained TEPA.

In the next step, the best capping agent were evaluated. For this purpose, PVP, PEG and SDS (Fig. 4) were investigated. As shown in Fig. 4a and 4b, the most appropriate morphology is obtained when the SDS used as a capping agent which nano-rod structure with narrow particle size distribution was obtained. Also PEG as capping agent produces nanoparticle with spherical morphology, but this nanoparticles are agglomerated and have larger size in the above conditions (Fig. 4c and 4d). By using of PVP as capping agent obtained the nanostructures with sheet-like morphology but the obtained particle size and particle distribution was larger in compare with when the SDS was used as capping agent (Fig. 4e and 4f). Therefore SDS and TEPA are better for preparation of $FeCr_2O_4$ nanostructure with uniform spherical shape and small grain size at 180 °C.

Now on the surface of the synthesized nanostructure using TEPA and SDS, which known as the optimum sample, silver nanoparticle was deposited by photodeposition method.

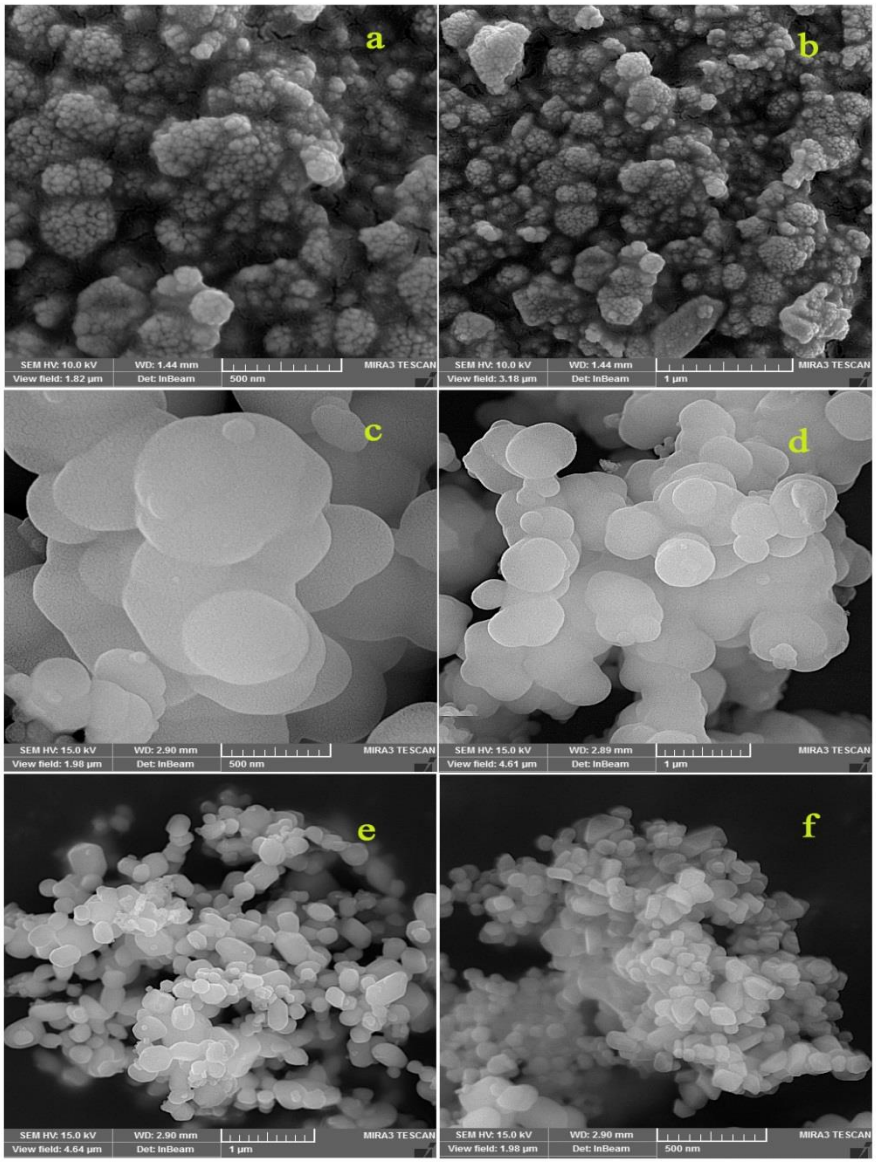

Fig. 3. FESEM images of the samples obtained by various alkaline agents; TEPA (a, b), $N(Et)_3$ (c, d) and NH_3 (e, f)

Fig. 5a and b depict morphology of $FeCr_2O_4$/Ag nanocomposite. As can be seen surface and size of $FeCr_2O_4$/Ag nanostructure (sample 7) is rough and elder in comparison with sample 4 nanostructure, which is evidence for coting of Ag particles on the surface.

To study the optical properties and to determine the band gap of the nanostructures, UV–Vis spectrum was applied. Optical band gap can be acquired using the following equation Eq. 2: $(\alpha h\nu)^n = B(h\nu - Eg)$ (2); Where hν is the photo energy, α is the absorption coefficient, B is a constant relative to the material and n is either 2 for a direct transition or 1/2 for an indirect transition. Fig.6a and b reveals the UV–Vis absorption spectrum of sample No.4 (prepared using TEPA in presence of SDS as capping agent) and 7 ($FeCr_2O_4$/Ag (2%)). The peaks nearly 242, 250, 258, 303, 326, 348, 378 and 395 nm (Fig. 6a) can be seen in the DR-UV-Vis spectrum of sample 4. The band gap can be explained based on the absorption spectrum using Tauc's equation. The band gap value of the sample 4 was achieved through extrapolating of the linear section of the plot $(\alpha h\nu)^2$ against hν to

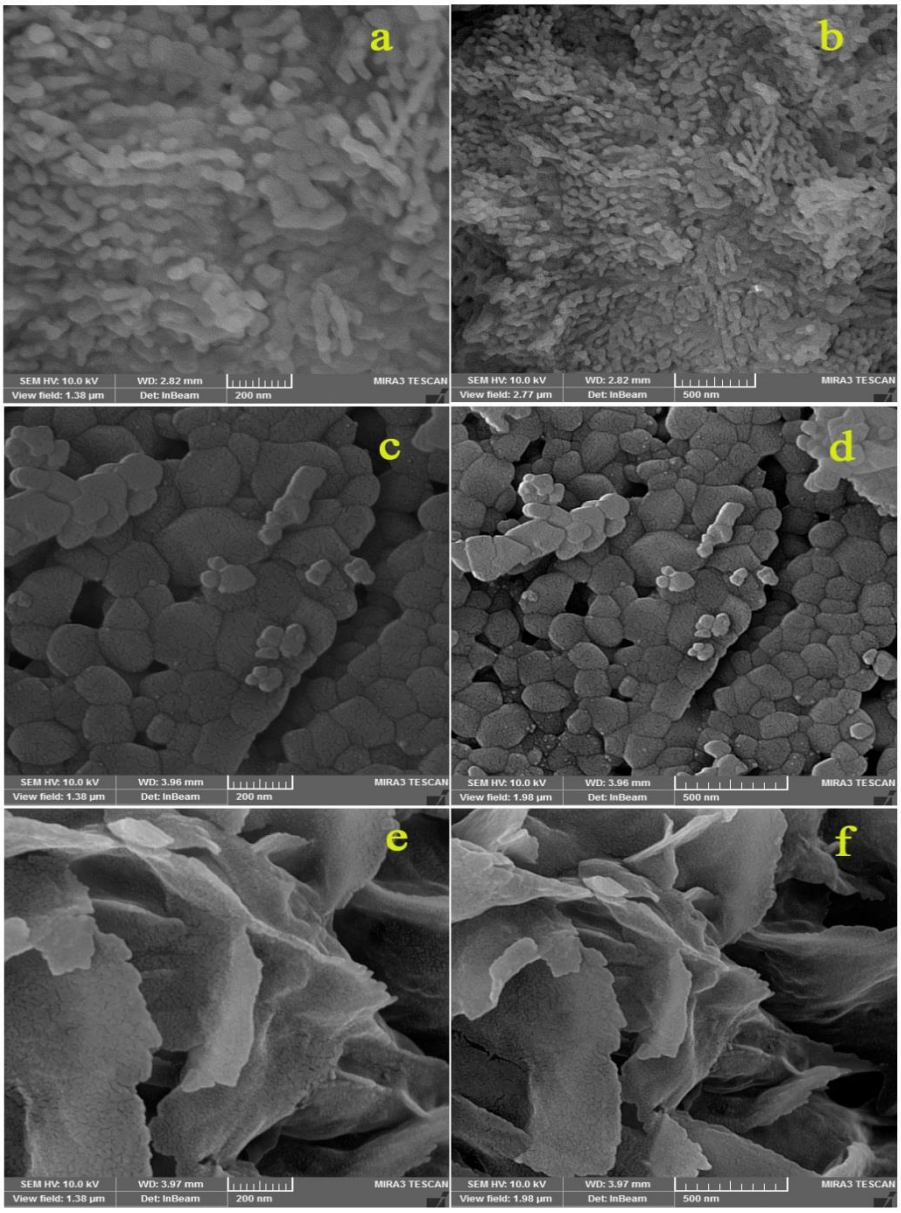

Fig. 4. FESEM images of the products prepared by different capping agents; SDS (a, b), PEG (c, d) and PVP (e, f)

the energy axis (Fig. 6c). The Eg value of the as-prepared $FeCr_2O_4$ nanostructures estimated to be 3.2 eV. Fig 6b shows absorption bands at 223, 244, 258, 279, 290, 306, 325, 341,398 and 405 nm for $FeCr_2O_4$/Ag nanocomposite. Fig. 6b reveals the UV–Vis diffuse reflectance spectrum of the $FeCr_2O_4$/Ag nanostructure. The Eg of the $MgCr_2O_4$/Ag nanostructure (sample no. 7) estimated to be around 3/08 eV (Fig. 6d). From the calculated Eg value, as-prepared $FeCr_2O_4$/Ag and $FeCr_2O_4$ samples may be employed as the photocatalyst under UV illustration.

The role of various capping agents and alkaline agent on the photocatalytic efficiency of $FeCr_2O_4$ has been investigated through monitoring the destruction of various dyes pollutant under ultraviolet illumination. The influence of various factors including kind of pollutant, grain size and morphology of FeCr2O4 nanoparticles and pH on photocatalytic activity of products were examined. Also the offered mechanism of the decomposition of dyes can be summarized as:

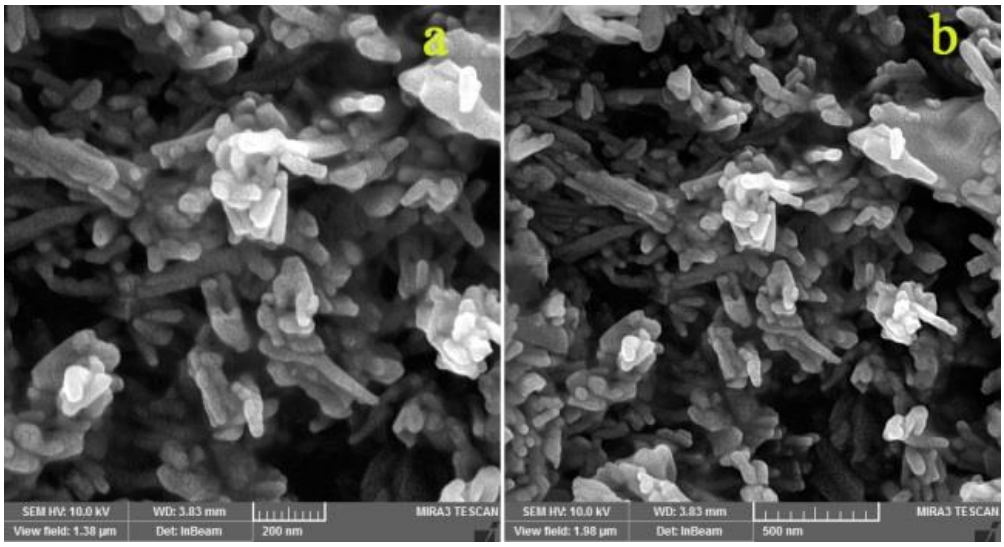

Fig. 5. FESEM images of $FeCr_2O_4$ /Ag nanostructures (sample 7)

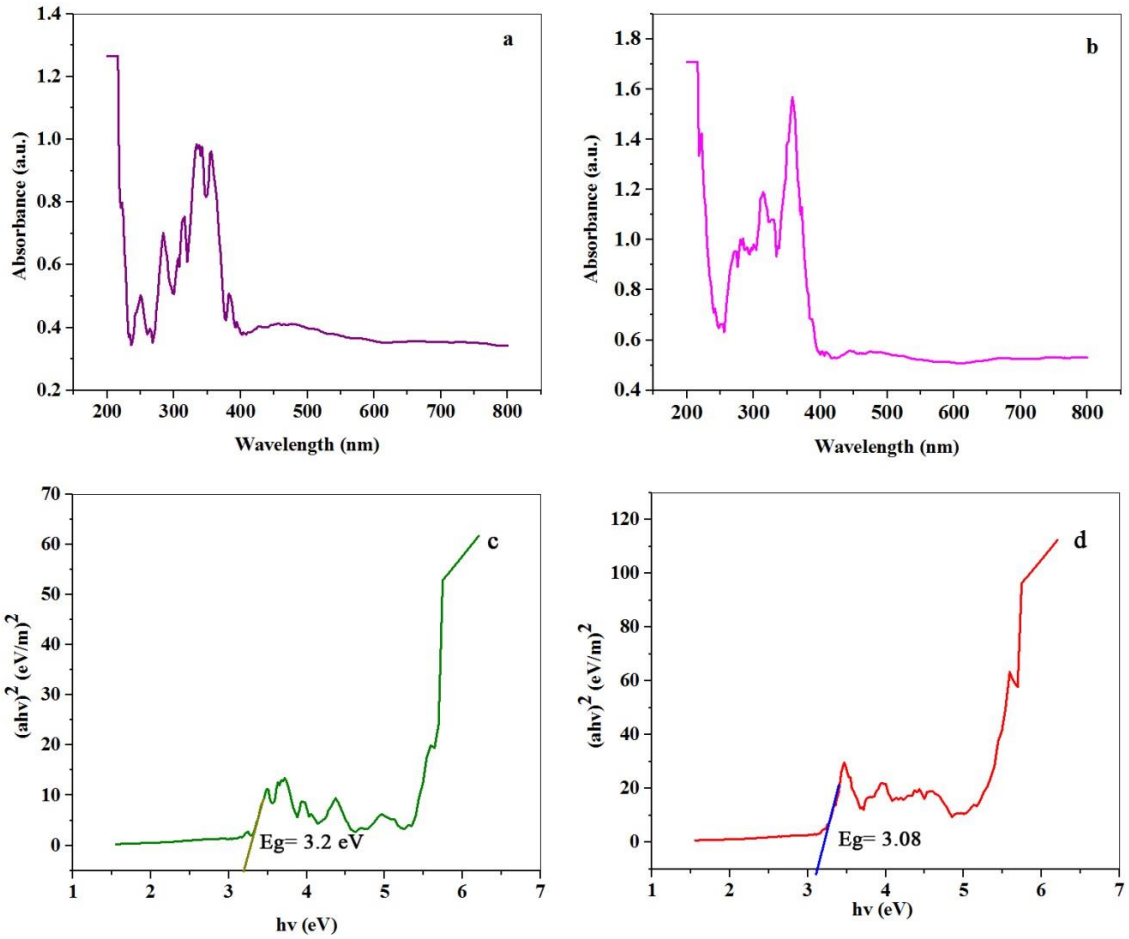

Fig. 6. UV–Vis diffuse reflectance spectrum and plot to determine the band gap of the $FeCr_2O_4$ (sample 4) (a and c) and UV–Vis diffuse reflectance spectrum and plot to determine the band gap of the $FeCr_2O_4$/Ag nanostructures (sample 7) (b and d)

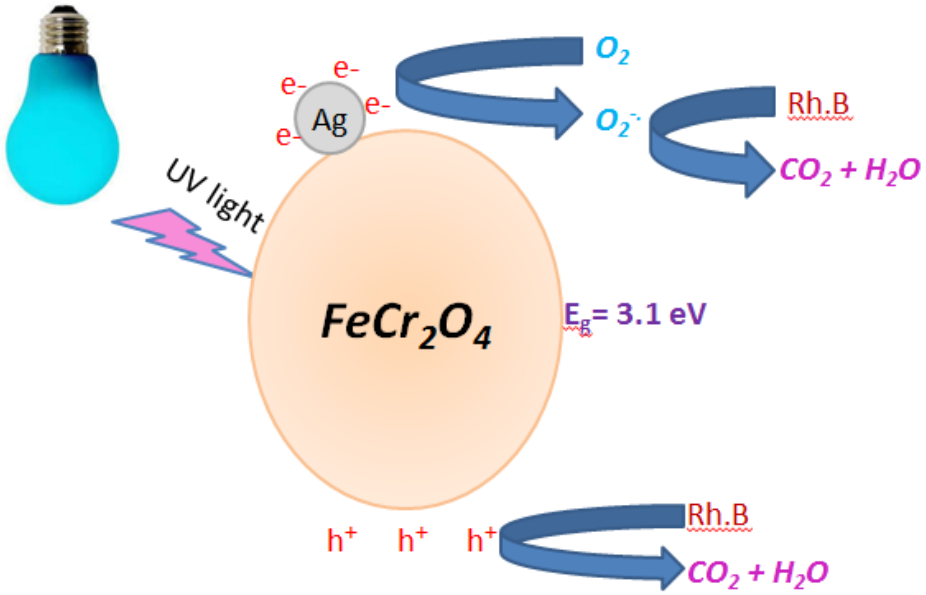

Fig. 7. Schematic diagram of the reaction mechanism of rhodamine B photodegradation by $FeCr_2O_4$/Ag

$FeCr_2O_4/Ag + hv \rightarrow FeCr_2O_4/Ag^* + e^- + h^+$

$h^+ + H_2O \rightarrow OH^- + H^+$

$2e^- + O_2 + 2H^+ \rightarrow O_2^{\cdot-}$

$OH^- + O_2^{\cdot-} + \text{Pollutants} \rightarrow \text{Destruction products}$

During the photocatalytic process, the generated electron and holes may migrate to the catalyst surface where they participate in redox reactions with adsorbed species. The h^+ may interact with H_2O to product the hydroxyl radical (OH^-). Also e^- may interact with O_2 to produce the oxygen radical ($O_2^{\cdot-}$). It has been suggested that the hydroxyl radicals (OH^-) and oxygen radical ($O_2^{\cdot-}$) are the essential oxidizing species in the photocatalytic perocess. For blank sample no dye degradation was observed after 70 min without using UV light irradiation or photocatalyst. In the base of this observation, the contribution of self-degradation is insignificant. The mechanism of decomposition of pollutants for the ferrite chromite product has been depicted in Fig. 7. As shown in this diagram, a photon can produces e^- and h^+ in conduction band and valence band of $FeCr_2O_4$/Ag respectively.

The photocatalytic activity of samples 4, 6 and 7 was evaluated for demolition of rhodamine B, the results are shown in Fig. 8. As it can be seen photocatalyst performance of sample 7 ($FeCr_2O_4$/Ag nanostructure) is much higher than that of samples 4 and 6. From the photocatalytic calculations, the rhodamine B contaminate destruction were about 52% by sample 4, about 61% sample 6 and about 69% by sample 7 after 70 min UV irradiation. By comparing the SEM images of as-prepared nanostructures (Figs. 4 and 5) it can be observed that the use of TEPA and SDS (sample 4) is satisfactory for the production of uniform spherical $FeCr_2O_4$ nanostructure. Because whatever the particle size is smaller the ratio of surface area to volume increases, therefore the catalytic performance is better. The photocatalytic activity of sample 7 ($FeCr_2O_4$/Ag) is better than other samples, because of two reasons; first, Ag particles were selectively deposited on the electron trapping sites in photodeposition process, so the resulting Ag particles will serve as new electron sumps to entrap electron and extract of them to demolition of dye. Second, it is generally admitted that the recombination of electron (e^-) and hole (h^+) has a significant impact on the photocatalytic performance. By decreasing the recombination of electron (e^-) and hole (h^+), the photocatalysis activity is increased. When the band gap decreases, the chance of recombination of electron (e^-) and hole (h^+) can be decreased, whereupon photocatalysis activity increases. In the case of nanostructured $FeCr_2O_4$/Ag with lower energy gap quantity then $FeCr_2O_4$, the electron and

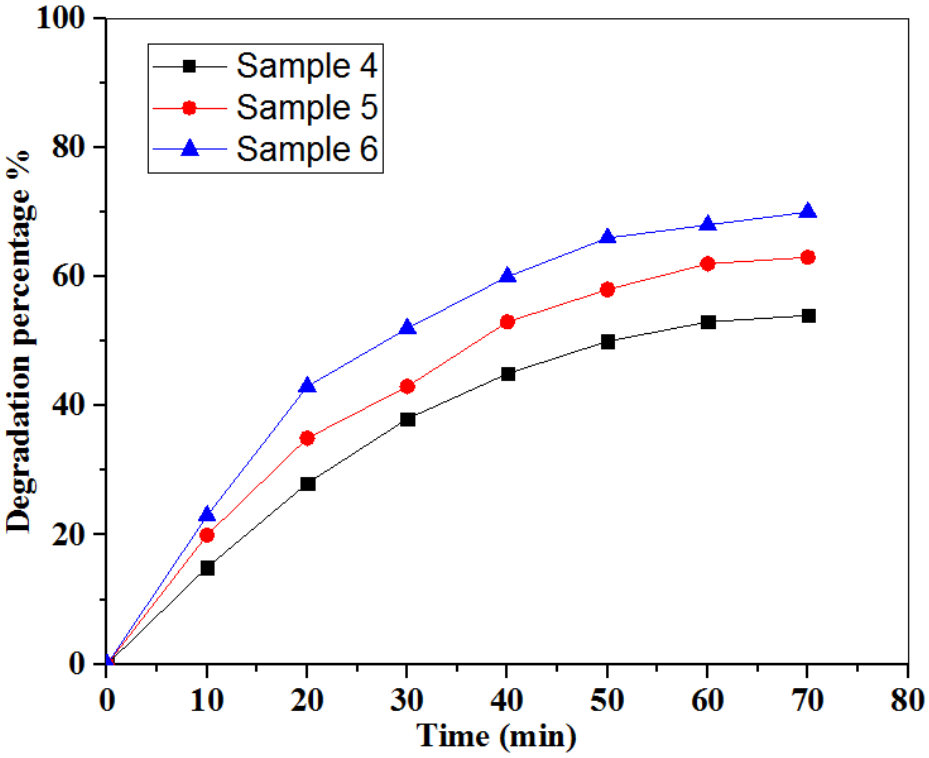

Fig. 8. The photocatalytic behavior of the as-prepared nanostructures (samples 4, 6 and 7)

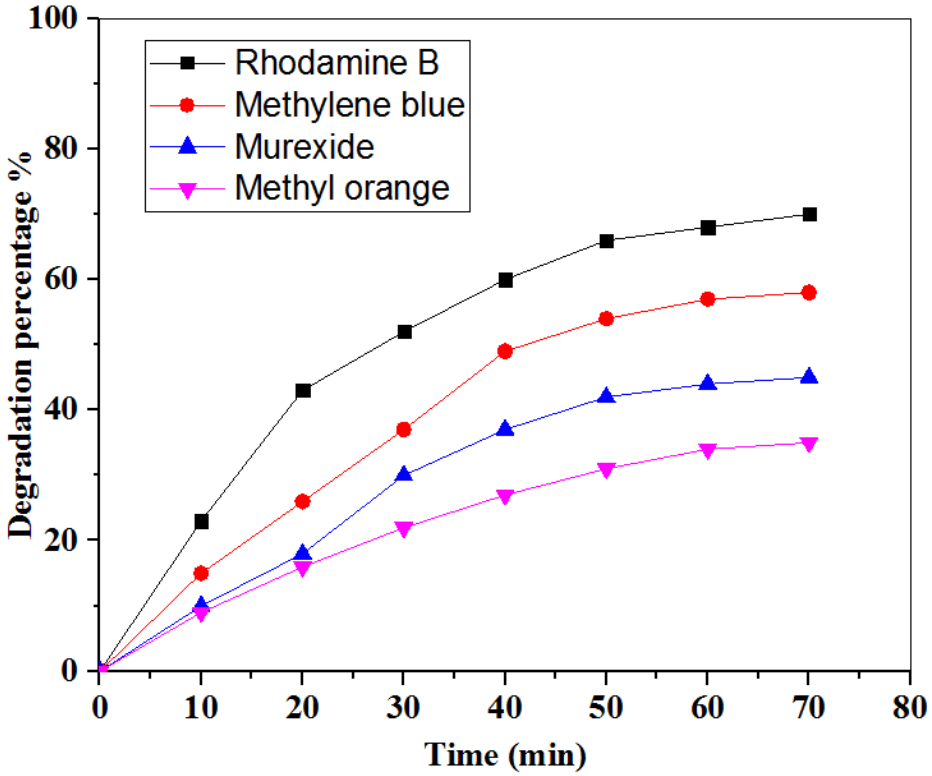

Fig. 9. The photocatalytic behavior of $FeCr_2O_4$/Ag nanostructures (sample 7) on decomposition of rhodamine B,methyl orange, methylene blue and murexide

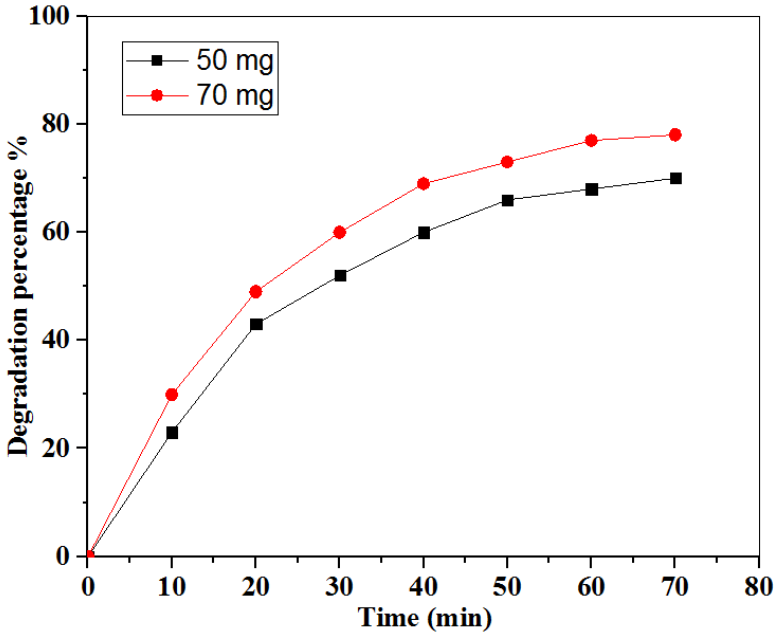

Fig. 10. The influence of the concentration of photocatalyst (sample 7) on the photocatalytic performance for degradation of rhodamine B

Table 1. The reaction conditions for synthesis of $FeCr_2O_4$ via a hydrothermal method

Sample No.	Alkaline agent	Capping agent	Temperature reaction	Ag-doped
1	$N(Et)_3$	-	180	-
2	NH_3	-	180	-
3	TEPA	-	180	-
4	TEPA	SDS	180	-
5	TEPA	PEG	180	-
6	TEPA	PVP	180	-
7	TEPA	SDS	180	2%

hole recombination is reduced and therefore the better photocatalytic performance is observed. In the next step, the photocatalytic performance of $FeCr_2O_4$/Ag was investigated for decomposition of Methyl orange, murexide and methylene blue, and the results were shown in Fig. 9. The catalysis efficiency of methyl orange, murexide and methylene blue are 34%, 44% and 56% respectively. It is evident that the photocatalytic destruction of anionic contaminants with a negative charge is weaker than cationic contaminants with a positive charge. The greatest amount of photocatalytic decomposition is for rhodamine B. These results reveal that in photocatalytic process, the cationic pollutant adsorption on the $FeCr_2O_4$/Ag is better than of adsorption of anionic contaminant on it. Forasmuch as the nanostructured $FeCr_2O_4$/Ag has oxygen atoms with a great electron density on its surface, it seems that $FeCr_2O_4$/Ag with negative charge can adsorb the cationic pollutant with positive charge. Fig. 10 reveals the effect of various amount of photocatalyst on the photocatalytic performance of $FeCr_2O_4$/Ag nanostructure. It can be seen that dye removal efficiency increased with the increase of photocatalyst concentration. The results illustrate that the percentage decomposition of rhodamine B under UV light increased from 69% to 76% with changing amount of photocatalyst from 50 to 70 mg in 50 ml of the contaminate solutions. The pH of the solution is known as effective parameter in the photocatalytic reactions. For investigate of the pH role on the destruction rate, two values of pH were tested. Destruction of rhodamine B

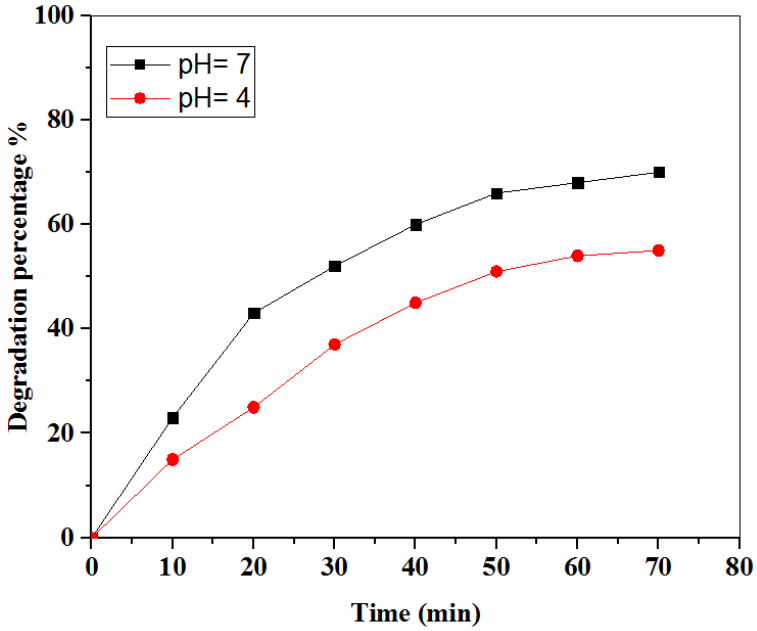

Fig. 11. Effect of pH on the photocatalytic decomposition of rhodamine B

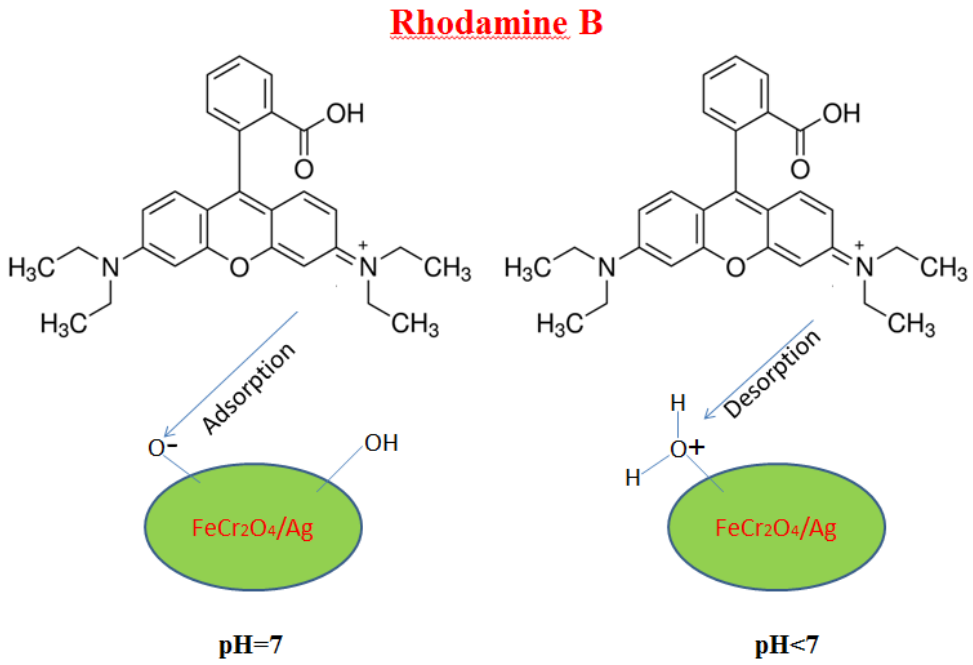

Fig. 12. Effect of pH on the adsorption and desorption rhodamine B on the surface of $FeCr_2O_4$/Ag nanostructures

was measured under acidic (pH=4) and neutral conditions (pH= 7) (Fig. 11). From photocatalytic calculations, the rhodamine B pollutant degradation was about 53% at pH= 5 and 69% at pH= 7 after 70 min UV illustration. By reducing pH, absorption of rhodamine B on the surface of the nanocatalyst is reduced. In acidic condition cationic molecules can be more desorbed on the surface. Subsequently, it can be seen that maximum demolition for rhodamine B was obtained in the neutral condition. Fig. 12 demonstrates in acidic conditions surface of particles has a lot of positive

charge and consequently cationic molecules are more likely to be desorbed from the surface.

CONCLUSION

In this work, $FeCr_2O_4$ nanostructures were prepared by hydrothermal method. The effect capping agent and alkaline agent were investigated on size and morphology of product. Results show that the best product has been achieved in presence of TEPA and SDS. In the next step, silver particle deposited on this pure nanoparticle. Results show that preparation conditions have been influenced on size and morphology of nanostructures and have the most important effect on the photocatalytic performance. The influences of various factors including kind of pollutant, grain size of $FeCr_2O_4$ nanostructures, amount of $FeCr_2O$/Ag and pH on photocatalytic activity of products were evaluated. It was observed that by using of $FeCr_2O_4$/Ag nanostructure instead $FeCr_2O_4$ nanoparticles the photocatalytic performance increased. Also results suggest that $FeCr_2O_4$/Ag nanoparticles are interesting and desirable candidate for photocatalytic applications under UV light.

ACKNOWLEDGEMENTS

The authors gratefully acknowledge the financial support provided by Iran National Science Foundation (Project 94019559).

CONFLICT OF INTEREST

The authors declare that there are no conflicts of interest regarding the publication of this manuscript.

REFERENCES

1. Zerr A, Miehe G, Serghiou G, Schwarz M, Kroke E, Riedel R, et al. Synthesis of cubic silicon nitride. Nature. 1999;400(6742):340-2.
2. Martinho H, Moreno NO, Sanjurjo JA, Rettori C, García-Adeva AJ, Huber DL, et al. Magnetic properties of the frustrated antiferromagnetic spinelZnCr2O4and the spin-glassZn1−xCdxCr2O4(x=0.05,0.10). Physical Review B. 2001;64(2).
3. Kim BN, Hiraga K, Morita K, Sakka Y. A high-strain-rate superplastic ceramic. Nature. 2001;413(6853):288-91.
4. Durrani S-K, Hussain M-A, Saeed K, Hussain S-Z, Arif M, Saee A. Synthesis and Sintering Studies of Magnesium Aluminum Silicate Glass Ceramic. Sintering of Ceramics - New Emerging Techniques: InTech; 2012.
5. Grazenaite E, Pinkas J, Beganskiene A, Kareiva A. Sol–gel and sonochemically derived transition metal (Co, Ni, Cu, and Zn) chromites as pigments: A comparative study. Ceramics International. 2016;42(8):9402-12.
6. Matulkova I, Holec P, Pacakova B, Kubickova S, Mantlikova A, Plocek J, et al. On preparation of nanocrystalline chromites by co-precipitation and autocombustion methods. Materials Science and Engineering: B. 2015;195:66-73.
7. Barbu M, Stefanescu M, Stoia M, Vlase G, Barvinschi P. New synthesis method for M(II) chromites/silica nanocomposites by thermal decomposition of some precursors formed inside the silica gels. Journal of Thermal Analysis and Calorimetry. 2011;108(3):1059-66.
8. Ghahfarokhi SS, Mamoory RS, Kalashami AG. Inverse precipitation synthesis of ZrO2 nanopowder and in-situ coating on MWCNTs. Ceramics International. 2018;44(12):13556-64.
9. Schüth F. Endo- and Exotemplating to Create High-Surface-Area Inorganic Materials. Angewandte Chemie International Edition. 2003;42(31):3604-22.
10. Stefanov P, Avramova I, Stoichev D, Radic N, Grbic B, Marinova T. Characterization and catalytic activity of Cu–Co spinel thin films catalysts. Applied Surface Science. 2005;245(1-4):65-72.
11. Fino D, Russo N, Saracco G, Specchia V. Catalytic removal of NOx and diesel soot over nanostructured spinel-type oxides. Journal of Catalysis. 2006;242(1):38-47.
12. Słoczyński J, Ziółkowski J, Grzybowska B, Grabowski R, Jachewicz D, Wcisło K, et al. Oxidative Dehydrogenation of Propane on NixMg1−xAl2O4 and NiCr2O4 Spinels. Journal of Catalysis. 1999;187(2):410-8.
13. Knyazev AV, Mączka M, Bulanov EN, Ptak M, Belopolskaya SS. High-temperature thermal and X-ray diffraction studies, and room-temperature spectroscopic investigation of some inorganic pigments. Dyes and Pigments. 2011;91(3):286-93.
14. Shangguan W. Simultaneous catalytic removal of NOχ and diesel soot particulates over ternary AB2O4 spinel-type oxides. Applied Catalysis B: Environmental. 1996;8(2):217-27.
15. Fino D, Russo N, Saracco G, Specchia V. Removal of NOx and diesel soot over catalytic traps based on spinel-type oxides. Powder Technology. 2008;180(1-2):74-8.
16. Wang YG, Wang YQ, Guo Y, Guo YL, Liu XH, Lu GZ. Mesoporous metal oxides and mixed oxides nanocasted from mesoporous vinylsilica and their applications in catalysis. Recent Progress in Mesostructured Materials - Proceedings of the 5th International Mesostructured Materials Symposium (IMMS2006), Shanghai, PR China, August 5-7, 2006: Elsevier; 2007. p. 361-4.
17. Słoczyński J, Janas J, Machej T, Rynkowski J, Stoch J. Catalytic activity of chromium spinels in SCR of NO with NH3. Applied Catalysis B: Environmental. 2000;24(1):45-60.
18. Mellor JR, Copperthwaite RG, Coville NJ. The selective influence of sulfur on the performance of novel cobalt-based water-gas shift catalysts. Applied Catalysis A: General. 1997;164(1-2):69-79.
19. Li S, Zhao G, Bi H, Huang Z, Lai H, Gai R, et al. Synthesis and anomalous magnetic properties of CoCr2O4 nanocrystallites with lattice distortion. Journal of Magnetism and Magnetic Materials. 2006;305(2):448-51.
20. Li S, Bi H, Tian Z, Xu F, Gu B, Lu M, et al. Surface spin pinning effect of polymer decomposition residues in CoCr2O4 nanocrystallites system. Journal of Magnetism and Magnetic Materials. 2004;281(1):11-6.
21. Dutta DP, Manjanna J, Tyagi AK. Magnetic properties of sonochemically synthesized CoCr2O4 nanoparticles.

Journal of Applied Physics. 2009;106(4):043915.
22. Rath C, Mohanty P. Magnetic Phase Transitions in Cobalt Chromite Nanoparticles. Journal of Superconductivity and Novel Magnetism. 2010;24(1-2):629-33.
23. Whipple E, Wold A. Preparation of stoicheiometric chromites. Journal of Inorganic and Nuclear Chemistry. 1962;24(1):23-7.
24. Cui H, Zayat M, Levy D. Sol-Gel Synthesis of Nanoscaled Spinels Using Propylene Oxide as a Gelation Agent. Journal of Sol-Gel Science and Technology. 2005;35(3):175-81.
25. Hu D-S, Han A-J, Ye M-Q, Chen H-H, Zhang W. Preparation and Spectroscopy Analysis of Spinel $CoCr_{2-x}Al_xO_4$ by Low-temperature Combustion Synthesis. Journal of Inorganic Materials. 2011;26(3):285-9.